
Article:
Wang, Tianyuan, Post, Mark Andrew orcid.org/0000-0002-1925-7039 and Tyrrell, Andy orcid.org/0000-0002-8533-2404 (2024) TWrist: An agile compliant 3-DoF tensegrity joint. Biomimetic Intelligence and Robotics. ISSN 2667-3797

https://doi.org/10.1016/j.birob.2024.100170

Biomimetic Intelligence and Robotics 4 (2024) 100170

Contents lists available at ScienceDirect

Biomimetic Intelligence and Robotics

journal homepage: www.elsevier.com/locate/birob

Research Article

TWrist: An agile compliant 3-DoF tensegrity joint

Tianyuan Wang *, Mark A. Post, Andy M. Tyrrell

School of Physics, Engineering and Technology, University of York, York YO10 5DD, United Kingdom

ARTICLE INFO

Article history:
Received 31 January 2024
Revised 27 May 2024
Accepted 26 June 2024
Available online 2 July 2024

Keywords:
Tensegrity
Soft robot
Tensegrity control
Robot manipulator

ABSTRACT

Tensegrity structures, with their unique physical characteristics, hold substantial potential in the field of robotics. However, the very structures that will give tensegrity robots potential advantages over traditional robots also hold long term challenges. Due to the inherent high redundancy of tensegrity structures and the employment of tension elements, tensegrity robots exhibit excellent stability, compliance, and flexibility, although this also results in lower structural deformation efficiency. Existing research has endeavoured to enhance the motion performance of tensegrity robots, exploring diverse approaches such as actuation schemes, structure design, aligned with control algorithms. However, the physical constraints of the elements in such structures and the absence of suitable controllers impede further advancements in the usefulness of tensegrity robots. This paper presents a novel design based on an under constrained transition region design and a tailored control approach based on inverse kinematics, improving the motion performance of the proposed novel tensegrity joint. Through this approach, the tensegrity joint, while preserving the advantages of compliance and flexibility expected from tensegrity structures, offers three degrees of rotational freedom, mirroring the controllability of conventional rigid-body joints. The results demonstrate the capability of tensegrity-based robotic joints to provide flexible actuation under situations demanding high compliance. The integration of structure design with a tailored control approach offers a pioneering model for future development of tensegrity robots, underscoring the practical viability of tensegrity structures in the realm of robotics.

1. Introduction

The deployment and application of robots in open, unknown environments represent longstanding challenges in robotics. Traditional robots, based on rigid structures, often struggle to meet specific requirements in certain application scenarios due to inherent limitations of their design. For example, planetary exploration missions impose high demands on the mass and mobility of robots, aiming to minimise launch and transportation costs while adapting to diverse terrains [1]. In post-disaster rescue operations, resilience to environmental hazards is crucial to withstand potential external impacts during operation [2]. In human–robot interaction scenarios, the compliance of robots during contact with humans ensures interaction safety [3]. In these contexts, soft robots, made from materials like rubber or silicone [4], demonstrate significant advantages. Their highly flexible structural materials enable multi-degree-of-freedom (DoF) movements, absorb substantial external impacts, and readily comply with external loads. However, these robots, in contrast to their rigid counterparts, sometimes approach another extreme of being overly soft. Although existing studies have made efforts to control stiffness [5,6], often soft robots can still compromise performance in tasks requiring high load-bearing capabilities and agile movements [4].

Conversely, tensegrity is a unique class of structures that differ from both traditional rigid structures and purely soft materials. It expands in three-dimensional space in an irregular and non-intuitive manner, arranging multiple repeating elements in equilibrium to form a cohesive whole. Comprising both rigid and flexible materials, tensegrity exhibits characteristics that lie between purely rigid and soft robots, embodying a structure that is both rigid and soft. It demonstrates advantageous characteristics in terms of mass efficiency, compliance, and robustness [7]. For the aforementioned scenarios demanding lightness, safety, and endurance, these advantages reveal the potential of introducing tensegrity to enhance the capabilities of existing robotic systems.

The term tensegrity was firstly coined by Buckminster Fuller [8] and appeared mainly in early stage artwork such as the X-Piece and Needle Tower [9]. Under a strict definition, it is described as a force-equilibrated structure consisting of continuous elements in tension and axially-loaded discontinuous elements in compression [10], which this paper refers to as *typical* tensegrity. Tensegrity structures are widely present in the natural world such as the spider silk [11–13], living cell

* Corresponding author.
E-mail address: tianyuan.wang@york.ac.uk (T. Wang).

https://doi.org/10.1016/j.birob.2024.100170

[14,15], and human body [11]. The early research and applications of tensegrity focused primarily on its static aspects, such as in civil engineering [8]. As research progressed, exploration began into the dynamic capabilities of tensegrity for applications in robotics. Driven by the demand for dynamic performance, variants emerged during this process, which this paper refers to as *atypical* tensegrity. Notable examples include the subcategory biotensegrity [16], inspired by the musculoskeletal system, where the compression elements are not necessarily axially loaded, and Class *k* tensegrity [7], where the compression elements can be non-continuous in the local region of the whole structure. For clarity, this paper adopts a broader definition that "tensegrity is a force-equilibrated structure consisting of continuous elements in tension and discontinuous elements in compression", where the condition "axially-loaded" is removed, since atypical tensegrity is widely employed in the robotic context.

The research on tensegrity robots initially focused on utilising their inherent structural characteristics, such as lightness, compliance, flexibility, and redundancy to enhance the robustness of robots without the cost of adding more mass. One of the pioneering studies in this field is the SUPERBall series robots conducted by NASA Ames Research Center [17]. Through actuating all or part of the tension elements in a tensegrity icosahedron [18,19], SUPERBall is able to achieve Entry, Descent and Landing (EDL) and locomotion on planetary exploration missions relying on the lander's own outer structure to actively deform and morph. After the robustness of tensegrity robots was widely recognised, research shifted towards how to achieve better movement with tensegrity structures. The icosahedron, as a typical representation of tensegrity structures, has been explored in various robotic studies, demonstrating diverse locomotion approaches such as crawling [20], rolling [17], and vibrating [21,22], showcasing the versatility of tensegrity in actuation schemes.

In addition to efforts in actuation schemes, current research has also explored more diverse forms of tensegrity structures, especially those based on atypical tensegrity. For example, the DuCTT series robots connect two tensegrity tetrahedrons, achieving agile movement and steering within pipes through the coordinated actuation of tension and compression elements [23,24]. The Laika robot employs a tensegrity spine composed of multiple stacked tetrapods, aiming to provide quadruped robots with more flexible body actuation capabilities [25]. The thin artificial muscle-driven tensegrity robot, which cascades tensegrity icosahedron modules of different functionalities, achieves worm-like movement in narrow spaces and multi-DoF maneuvers when anchored, revealing the flexibility of tensegrity-based robots in transitioning between roles as robot arms and mobile robots [20,26,27]. Tensegrity robots with similar stacked forms include Tetraspine and the 3-module soft robot [28,29]. Other studies have integrated continuous rolling motion into tensegrity locomotion, as seen in the spherical curved tensegrity robot [30], WTR [31], and MoTeR [32], aiming to enhance mobility by combining different modes of locomotion. Focusing from the whole robot down to the deformation of the structure, research devoted to actuating tensegrity structures, particularly for robot arm applications such as the bio-inspired tensegrity joint and the 3-DoF compliant tensegrity joint [33,34], demonstrates the large workspace, large number of degrees of motion freedom, and flexibility that tensegrity structures can offer for object manipulation.

As can be seen from the above, with a general consensus on the robustness advantages of tensegrity robots, current research in this field has a popular direction towards enhancing their agility, as aforementioned in efforts related to actuation schemes, structure designs, and control strategies.

However, problems remain. While tensegrity, as a unique structure, offers many advantages, it does not necessarily imply efficient movement. Contrarily, the complex and interconnected essence of tensegrity's parallel mechanism tends to under perform in this aspect. For a tensegrity structure, any change in a single element, mainly in length, will propagate through adjacent elements or even the entire structure, making its deformation difficult and increasing the complexity of control. Although one of the existing research approaches is to accept and utilise these characteristics, for certain applications, such as robot arms, the demand for agility makes this approach less suitable. As illustrated in the examples mentioned above, to meet the actuation requirements of robotic applications, a trend in tensegrity robot structure is the use of multi-segmented designs, amplifying the overall flexibility of the robot by stacking the movement of each segment. Despite making significant progress, this resembles more of an indirect approach, not fully overcoming the constraints of tensegrity's highly redundant parallel nature.

To address these challenges, the work presented in this paper has chosen to adopt a foundational approach, engaging in systemic thinking from the inside out. Concerning the existing tensegrity robots, their agility is mainly hindered in two aspects: first, the antagonistic motion among elements results in inefficient actuation; second, the overall structure's controllability, or predictability, remains low. Previous studies, as stated above, address these issues primarily through indirect approaches, which are a type of external compensatory method. Distinct from these approaches, this work introduces a concept called the under constrained transition region to the design of the tensegrity structure. It employs a substitutive scheme that modifies the structure from its root, purposefully reducing specific constraints within the structure. It thus provides designated degrees of freedom without compromising the integrity of the structure, where such an approach has not yet been seen in existing research.

Based on this, this paper presents a novel design of a compliant and flexible tensegrity robotic joint "TWrist". By cascading basic tensegrity triangular prisms based on an under constrained transition region design, this tensegrity joint is endowed with advanced torsional performance and provides three actuated degrees of rotational freedom at a single joint, which is well-suited for wrist joint applications. It is therefore possible to achieve a greater workspace with fewer segments when applied in a robot arm. The independence of each degree of freedom simplifies the complexity associated with conventional tensegrity structure deformation. The reduced motion antagonism among internal elements allows for the use of smaller actuators and achieving faster movement. This substitution-based approach offers a more direct and targeted solution distinct from existing approaches such as accommodating and utilising the characteristics, as that for SUPERBall [18,19], or circumventing them indirectly, as seen with the thin artificial muscle-driven tensegrity robot [20,26,27]. Compared to regular highly constrained stacked tensegrity structures, the joint achieves more agile movement while retaining the compliance and flexibility of tensegrity structures compared to conventional rigid ones.

The rest of the paper is organised as follows: Section 2 describes the design methodology of the tensegrity structure employed in the proposed robotic joint and the anticipated improvement in terms of motion of the structure. Section 3 presents the development of the prototype of the joint including the fabrication of the structure, the electronics design, and the control scheme. Section 4 presents the experiment and results with respect to the prototype joint's active workspace, passive compliance and agility, which is then discussed in Section 5. Section 6 presents the conclusions of the paper.

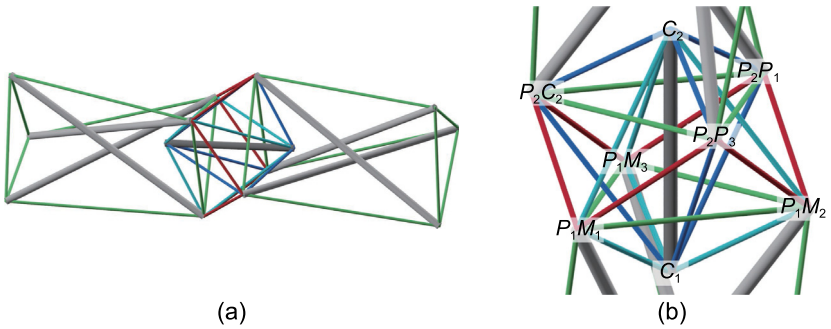

Fig. 1. Geometric model of the proposed robotic joint "TWrist". The rods are represented by light and dark grey cylinders. The passive cables are represented by green, cyan and blue cylinders. The active cables are represented by red cylinders. (a) The overview of the employed tensegrity structure design. (b) The detailed close-up of the joint with nodes labelled.

2. Tensegrity structure design

For clarity, in conjunction with existing definitions and classifications [7], this paper employs the following expanded classification:

> *A Class k tensegrity structure is a stable equilibrium of compression elements, with a maximum of k compression elements connected at the node(s).*
>
> *Compression elements of typical tensegrity consist of axially loaded rods only, whereas those of atypical tensegrity feature various geometries in two or three dimensions.*

The geometric model of TWrist is shown in Fig. 1. Given the classifications, TWrist is based on a typical Class 1 tensegrity structure. The reasons for using this type of structure are mainly two-fold:

(1) Although Class *k* tensegrity can to some extent reduce the complexity of topology, motion, and control of the structure by adding articulations between compression elements for robotics applications, Class 1 tensegrity provides better compliance and durability due to the complete elimination of direct contact between compression elements. This contributes to enhancing the robustness of the structure under harsh working conditions.
(2) While atypical tensegrity, targeting higher agility, is often incorporated into the design of tensegrity robots, using straight rods as compression elements in typical tensegrity can better leverage the strength of compression elements. This improves the mass efficiency of the structure, thereby reducing the inertia at the end-effector and enhancing agility.

TWrist generally adopts a cascaded 2-stage framework where each stage is composed of a basic tensegrity triangular prism. For consistency in description, the following naming convention is used: The robotic joint is vertically placed as that shown in Fig. 1(b) where the triangular faces of the prisms are parallel to the horizontal plane. Tension elements, i.e. cables, connecting nodes within the same triangular face are named as horizontal cables, while those connecting nodes in different triangular faces are called vertical cables.

A common approach for constructing stacked Class 1 tensegrity structures is to directly connect tensegrity segments end-to-end, as that for the Needle Tower [9] and the modular tensegrity arm [35]. The horizontal cables of the connected triangular faces are split in half, each connecting to the nodes of the prisms on the two sides. To maintain structural integrity, additional vertical cables are introduced to connect to the nodes on the distal side. Such multi-stage tensegrity structures are capable of offering properties similar with those of monolithic structures. However, the lower deformation efficiency, due to the highly redundant constraints imposed on the nodes, often limits its practical performance in robotic applications requiring high agility. In addition, as such a connection approach uses cables both for actuation and maintaining structural integrity, a loose state of cables caused by malfunction of actuators or inappropriate control inputs could lead to degradation of the structures' stability.

To mitigate the drawbacks of such a connection scheme, an intermediate tensegrity substructure based on the concept of an under constrained transition region (hereafter referred to as the transition region) is introduced to the connection of the prism segments of TWrist. The detailed geometric model of the transition region is shown in Fig. 1(b). To maintain a neutral posture in the absence of actuation, which is beneficial for assuring safety in robotic joint applications, the substructure is designed to apply minimal constraints to the twisting movement of the joint while imposing significantly more constraints to the tilt motion, resulting in one unconstrained degree of freedom. It consists of one central straight rod and 12 cables in total. The substructure does not hold structural integrity on its own but serves as part of the tensegrity structure to which it is connected. On one side, the nodes of the central rod (C_1C_2) are connected to the three nodes (P_1M_1, P_1M_2, P_1M_3) of the prism through three pairs of cables ($C_1-P_1M_1-C_2$, $C_1-P_1M_2-C_2$, $C_1-P_1M_3-C_2$) where on the other side it connects in a symmetrical manner. It is clear that based on such a topology, the transition region provides the two prisms it connects with free movement around its axial direction (C_1C_2) (hereafter referred to as the roll motion). The whole structure is capable of preserving the pretension condition of the cables when not actuated and thus maintaining the structural integrity. Without considering the physical volume of the rods and cables, it can provide a passive motion range of $\pm 60°$.

Regarding the tension elements in the structure, in addition to passive cables used to maintain structural integrity, six active tension elements are introduced to drive the degrees of freedom provided by the transition region. Inspired by the paradigm of tensegrity in the natural world, the musculoskeletal system, the active cables are arranged in a manner of antagonistic muscle pairs. During deformation, the movement of the active cables is complementary, imitating the contraction and relaxation of muscles during the flexion and extension of the human elbow. Therefore, in the actuated segment, where the distance between the nodes connected by the active cables changes, the active cables consecutively connect the adjacent nodes on two faces of the prisms, which are $P_1M_1 - P_2N_3$, $P_1M_2 - P_2N_3$, $P_1M_2 - P_2N_1$, $P_1M_3-P_2N_1$, $P_1M_3-P_2N_2$, $P_1M_1-P_2N_2$. This results in a similar configuration to the Stewart platform [36]. But unlike linear actuators, the active cables of tensegrity structure only provide

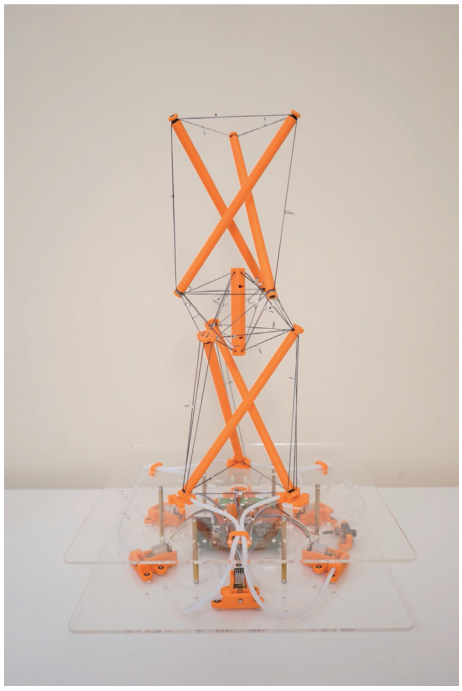

Fig. 2. The overview of the prototype of the proposed tensegrity joint TWrist. The 2-stage tensegrity structure which consists of two tensegrity triangular prisms and a transition region substructure is supported and driven by the stationary platform enclosing the electronics.

contraction motion. To drive the movement about a certain axis, it is necessary to tighten and loosen the adjacent active cables alternately. For example, to generate the clockwise roll motion of the joint, cables $P_1M_1 - P_2N_3$, $P_1M_2 - P_2N_1$ and $P_1M_3 - P_2N_2$ are to be tightened while cables $P_1M_2 - P_2N_3$, $P_1M_3 - P_2N_1$ and $P_1M_1 - P_2N_2$ are to be loosened, or vice versa.

Although the transition region only provides one unconstrained degree of freedom, owing to the configuration of the active cables and the compliance of the tensegrity structure, when simultaneously tightening adjacent active cables, the structure can generate the tilt movement (hereafter referred to as the pitch and yaw motion). In such situations, some of the passive cables will loose their pretensioned states but their role are to be replaced by the active cables to maintain structural integrity. Together with roll motion, the employed actuation scheme achieves active three degree of rotational freedom of the entire tensegrity structure.

3. Materials and methods

The prototype of TWrist is shown in Fig. 2. When implementing the tensegrity geometric model, several factors need to be considered such as the physical volume of the rods and cables, the approach for actuating the active cables and the control of the coordinated motion of the active cables. These are addressed and presented in the following subsections.

3.1. Assembly of tensegrity structure

TWrist is designed to be externally actuated to reduce the mass of the moving body. To realise this, it is mounted on a stationary platform containing the actuation devices. The platform is constructed with two layers of laser-cut acrylic plates. The bottom layer encloses the electronics, power supply and actuators for driving TWrist, while the top layer provides anchor points for fixing the bottom nodes of the tensegrity prism onto the platform.

There are two types of rods with different length and diameter for the compression elements of the tensegrity structure, both printed with polylactic acid (PLA) material (eSUN PLA+ Filament 1.75 mm Orange). The longer rod with smaller diameter is used to construct the tensegrity prisms, while the shorter but thicker rod is used for the central rod of the transition region.

Each long rod is 210 mm in length and 10 mm in diameter. As shown in Fig. 3(a), there are U-shaped circular grooves near both ends of the rod to secure the cables, set at a distance of 200 mm apart. As the rods are 3D printed vertically, the layer adhesion and the presence of grooves reduces the strength of the rod to radial tension forces exerted by the cables. Therefore, at the end of the rod, a 10 mm M3 screw is introduced for reinforcement. The cables are tied to the grooves using the girth hitch. Attaching cables to the grooves allows for rotation of the cables around the rod, eliminating the twisting forces on the non-axial direction of the rod that are commonly seen with through hole based fixation methods, which could lead to additional assembly errors and increase the deviation between the real tensegrity structure and the geometric volume-less model.

In contrast to the long rods of the prisms, the central rod (92 mm length, 15 mm diameter) of the transition region employs a different design, incorporating fixed-angle cable-guiding slots to restrict the rotational movement of the cables around the rod to a fixed level. As shown in Fig. 3(b), there are six equally spaced slots at the end of the central rod for cable guidance and rotation restriction. The cables from the central rod to the prisms are firstly wrapped around the inner circular groove and then exit through the guide slots. Based on this design, it retains a neutral posture in terms of the rotation about the axial axis of the adjacent triangular faces of the two prisms when the active cables are in loose states or not present, ensuring a symmetry for maximum roll motion range. Additionally, as the cables are pretensioned, the joint will also automatically return to the neutral posture in terms of the pitch and yaw motion in passive manner, ensuring the structural integrity and stability as per the geometric design anticipated.

The tension elements of the tensegrity structure are made up of fishing lines and also have two different types: the monofilament single strand Nylon line (Seaknight BLADE Nylon Fishing Line 35 LB 0.5 mm) for passive cables, and the multifilament braided Polyethylene line (HERCULES Braided Fishing Lines 8 Strands 90 LB 0.5 mm) for active cables. The former is used throughout the tensegrity structure to provide passive structural integrity. Compared to the braided line, the single strand line offers higher elasticity for better compliance and flexibility of the joint. The latter, with its higher longitudinal stiffness and bending softness, is used for active cables to improve the precision of length control.

As tensegrity is compliant and flexible owing to the elasticity of its cables, to minimise assembly errors, especially those introduced during the cable tying process, the cables are prefabricated with several fixed lengths in this study. The terminals of each cable are secured with a 0.5 mm aluminium crimp. The passive cable connects the rods on its ends with double lines, while the active cable uses single line to connect the rod and the actuator.

As the active cables of TWrist are driven by external actuators, to avoid introducing additional load paths into the structure, the active cables are designed to have a coincident path with the passive cables within the non-actuating section. Therefore, to guide the active cables through these non-actuating path, six end caps are installed at both ends of the rods of the lower prism to provide a turning point for changing cable direction at the nodes. For the non-actuating path from the actuator to the tensegrity structure, they are guided by Polytetrafluoroethylene (PTFE) tubes. On one

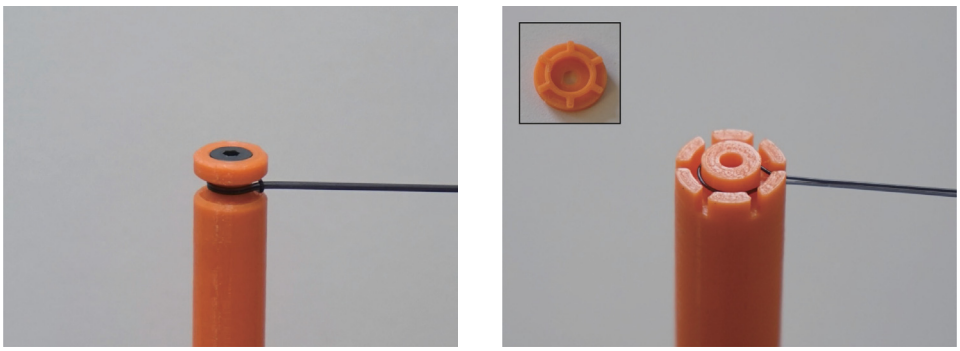

Fig. 3. The illustration of two fixation methods of cables to rods. (a) The girth hitch tying the cables to the circular groove of the long rod, allowing the cable to rotate about the rod. (b) The cable wrapped on the inner circular groove of the short rod and exit through the guide slot, preventing the relative rotation. The short rod comes with end caps which is depicted on the upper left corner.

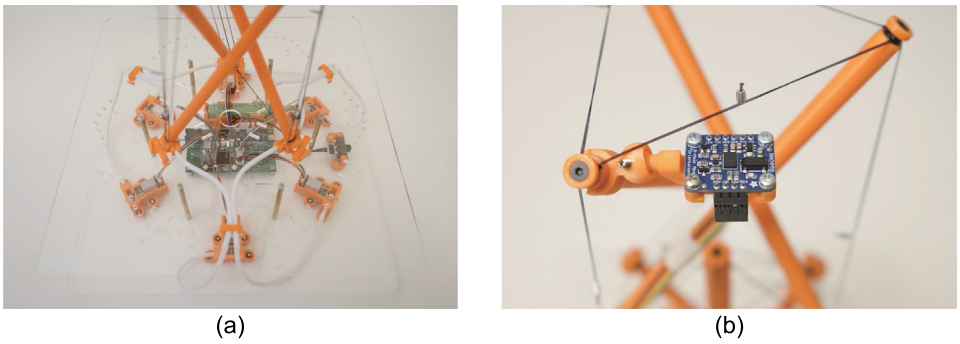

Fig. 4. The close-up of the electronic system of the TWrist prototype. (a) The stationary platform containing devices for control, power and actuation for the system. (b) The orientation sensor mounted on the upper tensegrity prism for posture measurement.

side, the PTFE tubes are fixed perpendicularly to the actuator output shaft, and on the other side they are fixed to the bottom end caps. The bottom end caps are also used for mounting TWrist prototype onto the top layer of the stationary platform.

3.2. Electronics

The electronic system of TWrist consists of an integrated control board, six geared DC motors (Pimoroni 110:1 Micro Metal Gearmotor extended back shaft with 12 CPR encoder), a lithium-ion battery cell (LG INR18650MJ1 3500 mAh), and an orientation sensor (Adafruit BNO055 absolute orientation sensor module), as depicted in Fig. 4. The control board is composed of a microcontroller (STM32F417), three motor drivers (TB6612), three boost converters (FP6291) providing 6 V power rail for the motor drivers, a linear regulator (ASM1117) regulating a voltage of 3.3 V for the microcontroller, three battery chargers (TP4056) for charging up to three battery cells, and a USB to UART bridge (CP2102). The onboard system is managed by the STM32. It is responsible for controlling the motors to change the length of the active cables at a frequency of 100 Hz based on the control algorithm and the desired joint posture. The active cables are actuated by using the motors as winches. The output shaft of each motor is drilled with a hole perpendicular to its axial direction for cable fixation and acts as the drum of the winch. Each pair of motors is driven by one motor driver, operating with a 20 kHz PWM signal provided by the microcontroller. The microcontroller is also responsible for establishing bidirectional communication with the host computer through the UART communication to receive commands and report back various data. Finally, it handles the storage of system status information.

The orientation data were acquired from the BNO055 module, which is mounted on one of the rods of the upper tensegrity prism through a holder with a spherical joint, as illustrated in Fig. 4(b).

3.3. Control algorithm

The inherent multi-degree-of-freedom feature of tensegrity structures brings advantages to their robotic applications but concurrently poses challenges in their control mechanisms. A prevalent approach involves approximating the comprehensive continuous deformation through an integration of binary control with an array of controlled elements.

In the case of TWrist, a distinctive actuation approach simplifies the structure's deformation control process, facilitating operations that are continuously controllable. The tensegrity structure of TWrist is a parallel mechanism in its essence. Its actuator parameter is the length of each active cable, which is in contrast to the joint angle for common serial manipulators. Given that TWrist is endowed with three active degrees of rotational freedom but not translational movement, this study employs intrinsic roll-pitch-yaw Euler angles as control inputs for its Inverse Kinematics (IK). Assuming the lower prism is fixed and the coordinate system's origin is coincident with the centre of the joint, it is commonly given as follows for a joint with single pivot point.

$$\boldsymbol{N}_{i\,new} = \boldsymbol{R}_{ZXY}\boldsymbol{N}_{i\,neutral}, \quad i \in \{1, 2, 3\} \tag{1}$$

with

$$\boldsymbol{R}_{ZXY} = \begin{bmatrix} c_1c_3 + s_1s_2s_3 & c_3s_1s_2 - c_1s_3 & c_2s_1 \\ c_2s_3 & c_2c_3 & -s_2 \\ c_1s_2s_3 - c_3s_1 & c_1c_3s_2 + s_1s_3 & c_1c_2 \end{bmatrix}$$

$$\boldsymbol{l}_j = |\boldsymbol{N}_{i\,new} - \boldsymbol{M}_k|, \quad i,k \in \{1,2,3\}, \quad j \in \{1,\ldots,6\} \tag{2}$$

where $\boldsymbol{N}_i$ is the position of the bottom nodes of the upper prism, $\boldsymbol{M}_k$ is the position of the top nodes of the lower prism, and $\boldsymbol{l}_j$ is the length of the active cables connecting $\boldsymbol{N}_i$ and $\boldsymbol{M}_k$. $\boldsymbol{R}_{ZXY}$ is the rotation matrix. c and s are the abbreviations for *cos* and *sin* respectively. The subscripts 1, 2 and 3 denote the angles following the Z-X-Y sequence respectively.

However, since cables only provide contraction forces, providing no expansion forces on the flexion side for the pitch and yaw motions, the pivot point deviates from the centre of the joint at these motions. A two-step control methodology is thus introduced to determining the length of each active cable for a desired joint orientation.

The initial step addresses the unconstrained roll motion, where the rotation is centred around the axial axis of the central rod in the transition region. The coordinates of the nodes $\boldsymbol{N}_i$ as an intermediate step can be calculated given the desired roll angle as that in Eq. (3).

$$\boldsymbol{N}_{i\,intermediate} = \boldsymbol{R}_Z \boldsymbol{N}_{i\,neutral}, \quad i \in \{1,2,3\} \tag{3}$$

where $\boldsymbol{R}_Z$ is the rotation matrix denoting the roll motion.

The subsequent step involves firstly determining the new orientation vector of the upper prism's longitudinal axis using the designated pitch and yaw angles. By projecting the orientation vector onto the horizontal plane passing through the centre of the central rod, a 2D vector is obtained, as given in Eq. (4) and (5).

$$\boldsymbol{V}_{tilt} = \boldsymbol{R}_{XY} \boldsymbol{V}_{neutral} \tag{4}$$

$$\boldsymbol{V}_{tilt}(x,y,z) \rightarrow \boldsymbol{d}(x',y') \tag{5}$$

with

$$x' = \frac{x}{\sqrt{x^2+y^2}}, y' = \frac{y}{\sqrt{x^2+y^2}}$$

where $\boldsymbol{V}$ denotes the centre of the upper prism top face, representing the orientation of the upper prism after the pitch and yaw motions. $\boldsymbol{R}_{XY}$ is the combined pitch and yaw rotation matrix. $\boldsymbol{d}$ is unit vector of the projection of $\boldsymbol{V}$ on the horizontal plane.

The intersection $\boldsymbol{P}_{pivot}$ of the projected vector $\boldsymbol{d}$'s extension line in the opposite direction with the inscribed circle of the regular hexagon of active cables' projection at the neutral posture on the horizontal plane is then computed as that in Eq. (6), with an illustrative graph shown in Fig. 5.

$$\boldsymbol{P}_{pivot} = -r\boldsymbol{d} \tag{6}$$

where r is the radius of the inscribed circle.

Utilising this intersection as a pivot point, combined with the coordinates of nodes obtained in the initial step as starting parameters, the rest of the IK is applied to derive the final node coordinates and thus the lengths of the active cables are determined as shown in Eq. (7) and (8).

$$\boldsymbol{N}_{i\,final} = \boldsymbol{R}_{XY}(\boldsymbol{N}_{i\,intermediate} - \boldsymbol{P}_{pivot}) + \boldsymbol{P}_{pivot}, \quad i \in \{1,2,3\} \tag{7}$$

$$\boldsymbol{l}_j = |\boldsymbol{N}_{i\,final} - \boldsymbol{M}_k|, \quad i,k \in \{1,2,3\}, \quad j \in \{1,\ldots,6\} \tag{8}$$

To improve the precision of control, this approach uses the actual coordinates of the active cables' turning points of the prototype based on the end caps' geometry for calculation, rather than the node coordinates in the geometrical model. In addition, the use of braided fishing lines with a high longitudinal stiffness for the active cables reduces the demand for pretensioning and it is therefore not introduced in this control approach.

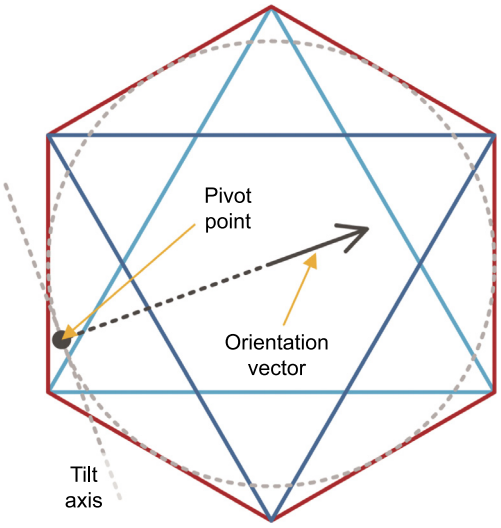

Fig. 5. The illustrative graph for the calculation process of the pivot point of pitch and yaw motions. The red, cyan and blue solid lines represent the active cables, passive cables connecting the lower prism and the central rod, and the passive cables connecting the upper prism and the central rod, respectively. The black arrow represents the projection of the orientation vector on the horizontal plane passing through the centre of the structure. The black point represents the resultant pivot point.

3.4. Simulation environment

In this study, certain experiments were conducted within a simulation environment. These include the collection of node coordinate data and the measurement of tension in the active cables during movement. The simulation is based on Chrono Engine, a multi-physics dynamics simulation engine with validated fidelity [37,38]. The modelling in the simulation replicated the dimensions, materials, control method, and experimental procedures of the TWrist prototype. The cables were modelled using finite element analysis (FEA) objects with Absolute Nodal Coordinate Formulation (ANCF) to handle large changes in cable length. The rods were constructed as rigid bodies without considering the bending, buckling and yielding. Since the experiments did not involve interactions with environmental objects, collision detection was disabled. The simulation was configured with a time step of 0.001 s using the "PardisoMKL" solver and the "Euler Implicit Linearized" time stepper provided by Chrono Engine. Two models were created for the simulation: a replica of TWrist and a typical stacked tensegrity joint. These are depicted in Fig. 6 in their neutral posture.

4. Experiment and result

To assess the efficacy of the proposed tensegrity robotic joint, particularly its capability to maintain stability and compliance while providing effective manipulation, this study conducted the evaluation of TWrist's active workspace, its deformation under external loads, and the required forces for actuation. Fig. 7 illustrates the prototype in its neutral posture, along with active roll, pitch, and yaw postures, as well as passively induced pitch and yaw postures.

4.1. Active workspace

Since the active degrees of freedom of TWrist are all rotational motion, the array of attainable end-effector postures resembles a domed shape. For a more intuitive workspace evaluation, the

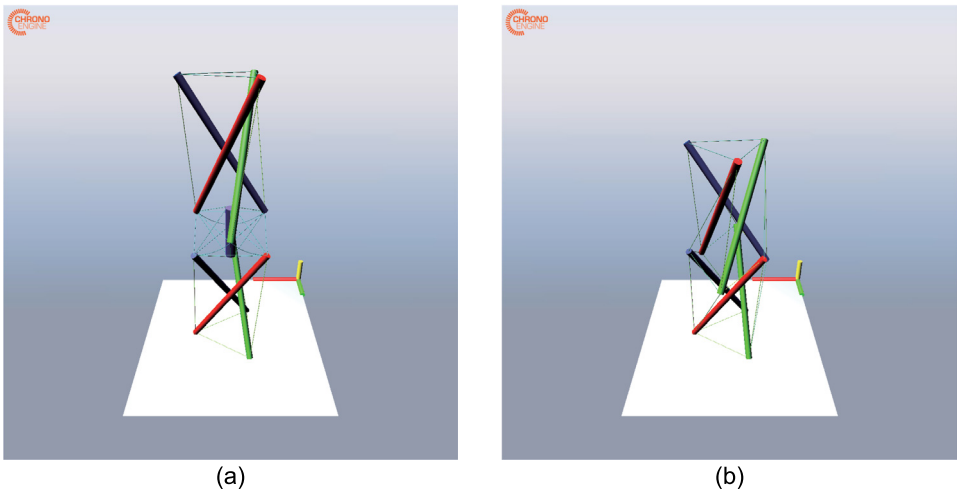

Fig. 6. The rendered scene of the simulation. (a) The simulation model of TWrist. (b) The simulation model of the tensegrity joint based on a typical tensegrity tower design.

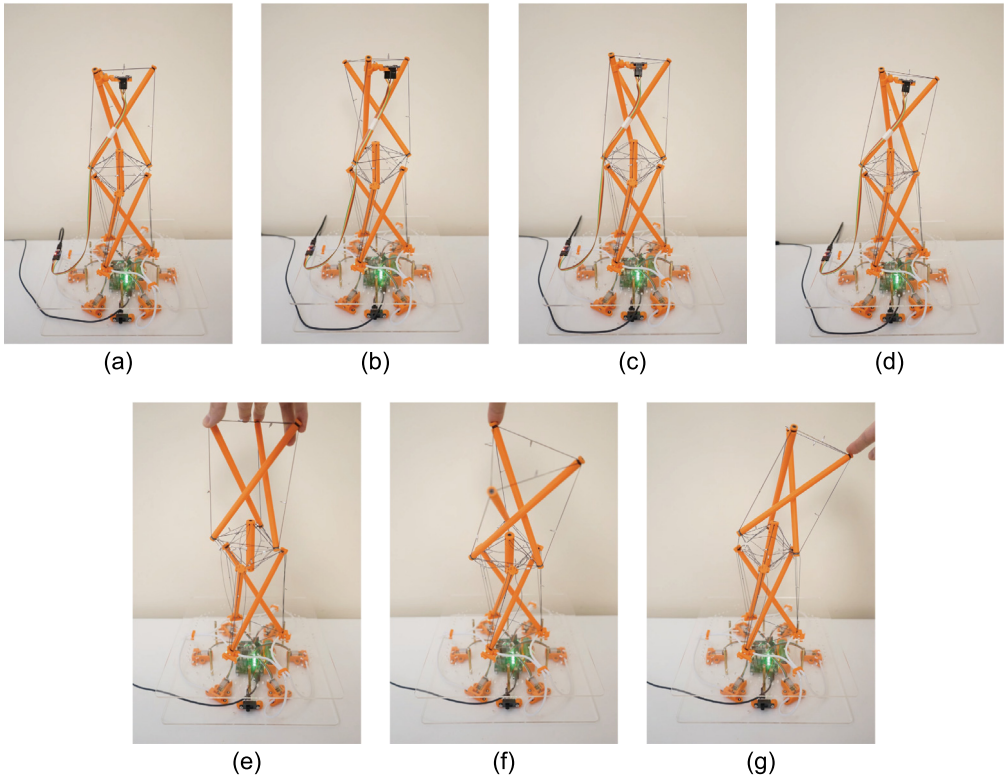

Fig. 7. The prototype of TWrist in different postures. (a) The neutral posture. (b-d) The active roll, pitch and yaw motions, respectively. (e-g) The passively induced roll, pitch and yaw motions, respectively.

maximum motion ranges for each of the three degrees of freedom were quantified. Due to practical constraints such as the inherent flexibility of the structure, position of the cable guides, cable frictions, and the maximum motor output, the prototype will not be able to reach the geometric model's theoretical limits, especially for pitch and yaw motions. The test ranges for all motions were set at $\pm 20^\circ$ for consistency. The measurements were conducted through a series of slow, quasi-static movements, with the control unit receiving desired postures at approximately 100 Hz. Each motion cycle, encompassing reciprocation movement of individual degree of freedom starting from the neutral posture, lasted 80 s, interspersed with 20 s rest periods. Fig. 8(a) illustrates the prototype's time-series data of this test motion sequence.

It can be seen that the joint's performance in roll motion closely aligned with the anticipated profile, achieving a peak output of around 16°. After the roll sequence is completed, a deviation of approximately 3° from the starting position was observed, highlighting the imprecision and hysteresis inherent in such soft robotic joints. Similar patterns were noted between pitch and yaw motions, with actual maximum angles of about 7.5° to 10° against a 20° input. Compared with the roll motion profile, near-extreme profiles of the pitch and yaw movements exhibited gradual curves rather than sharp transitions. This is consistent with the design intent. The transition region's small constrain along the axial axis facilitated the enhanced agility for roll motion, whereas for pitch and yaw movements, typical

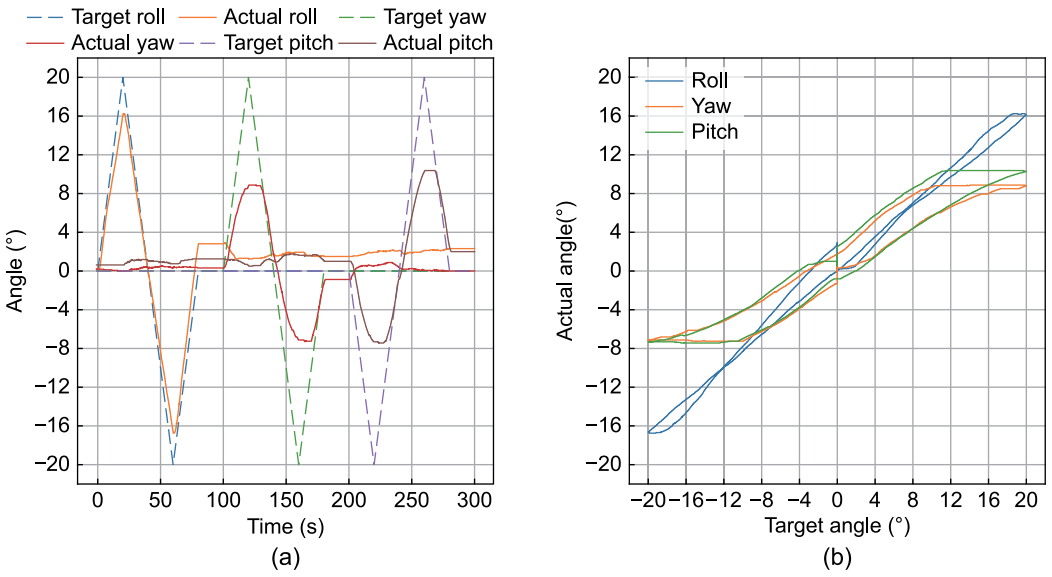

Fig. 8. The results of the active workspace experiment. (a) The time series of the target and observed angles of each motion with respect to time across the test sequence. (b) The comparison between the target and observed angles.

constraints were retained to preserve radial load-bearing efficacy without the involvement of active cables.

The results reveal that the error of TWrist's movement is higher compared to conventional rigid joint. However, it is important to note that for tensegrity, as a type of soft structure, characterised by high compliance and flexibility, this is within expectations. Meanwhile, to better characterise TWrist, real-time posture feedback is not included in the control loop while the low level actuation of active cables is. One primary reason for the large error is that, the elements of TWrist are highly interconnected. The IK employed does not account for the deformations of elements other than the active cables. Therefore, the structure deformation caused by passive elements during the actuation of active cables partially counteract the intended movement. This is more obvious in pitch and yaw motions due to higher internal constraints compared to the roll motion. Fundamentally, this is due to a lack of complete numerical model of TWrist's tensegrity structure. However, constructing a comprehensive model and having a simulated replica during the operation of such a soft structure is not deemed an effective approach in practice. Secondly, the fabrication and calibration of the tensegrity structure can introduce large errors. For example, during the fabrication of the cables and their attachment to the ends of rods, maintaining consistent relative positions between nodes as defined by the control model is challenging, especially without a motion capture system for calibration. In fact, research on tensegrity robots does not normally explore motion accuracy but focuses on demonstrated capabilities such as compliance, movement speed, and workspace. The evaluation of control precision in TWrist is mainly owing to its intended application scenarios centring around robot arms. Potential solutions for improving the accuracy of TWrist are discussed in Section 5. Despite the large errors compared to conventional rigid-body joints, the experiments showcased the joint's improved maneuverability under the proposed control scheme, especially when comparing the roll motion performance with those of pitch and yaw.

Fig. 8(b) shows a comparison between the expected and actual motion angles. It reveals a common characteristic across different degrees of freedom that the non-overlapping departure and return trajectories roughly forms closed loops, indicating hysteresis in TWrist's motion. This aligns with the material properties of the

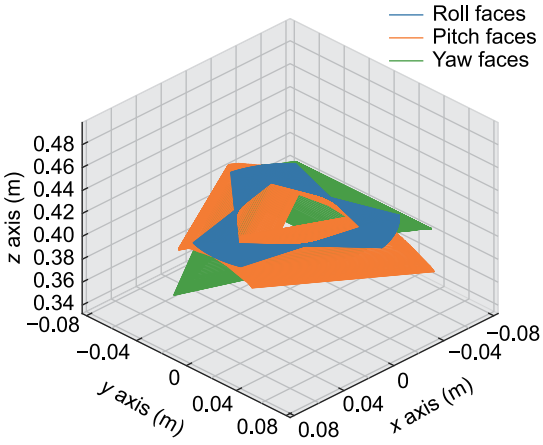

Fig. 9. The locations of the upper prism's top face for the active workspace experiment, with each motion represented by a distinct colour.

elastic cables and the constitute structures. However, characterising such traits for the joint requires additional effort to enhance precision in practical applications.

To intuitively illustrate the workspace of a robotic joint, motion capture systems are commonly employed to sample the end-effector positions. However, given the limitations imposed by the small size of the TWrist prototype and the experimental resources, this paper utilised simulation as an alternative. Due to the challenges associated with modelling intricate details such as cable bends and knots, the simulation implemented reasonable simplifications, including adjustments for anchor point offsets caused by tying cables to rods. The workspace of TWrist was depicted by recording the coordinates of the three nodes on the upper prism's top face, as presented in Fig. 9.

It is worth mention that, as a multi-DoF robotic joint, it is necessary to analyse the singularity and null space of TWrist. With its single-joint, 3-DoF design, TWrist shares certain characteristics akin to a 3-DoF gimbal, where singularities typically occur when its rotation axes coincide. The difference is that, due to the introduction of parallel actuation scheme and its specific rotational range of each DoF, TWrist is not subjected to such cause

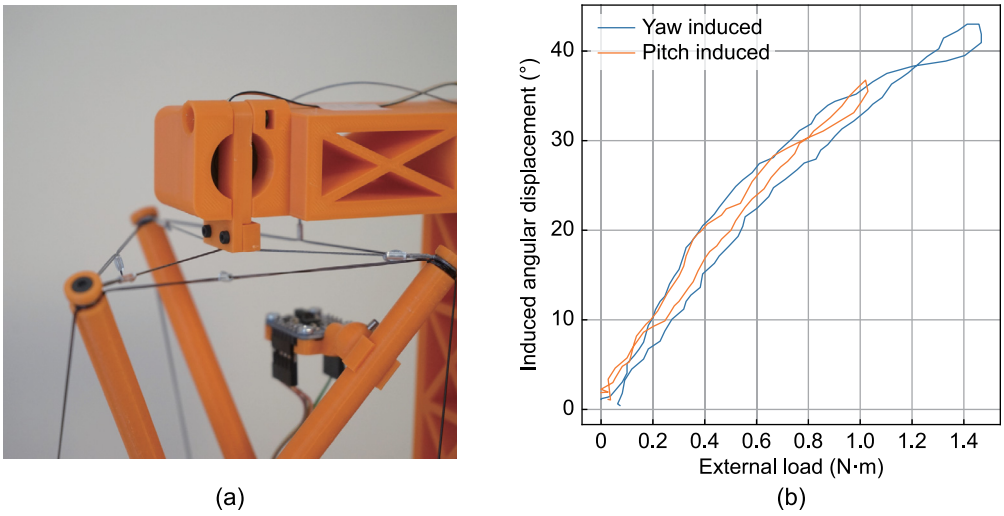

Fig. 10. The compliance experiment setup and results. (a) The close-up view of the trifurcated cable knot connected to the dynamometer for measuring the force applied to TWrist. (b) The induced pitch and yaw motion of the TWrist prototype based on external loads applied in the radial directions.

of singularity. Instead, its mobility could be compromised when it is at the extremes of its movement range. In fact, these are more limits of the workspace rather than kinematic singularities. However, when looking into the control algorithm employed for TWrist, it can be seen that despite being a single-joint mechanism, the IK of TWrist are not based on a single pivot point. This leads its singularity analysis analogous to that of a 2-DoF serial robot arm, where the first joint rotates in the horizontal plane about z axis and the second joint rotates vertically at the end of the first segment, that is, about a local horizontal axis depending on the orientation of the first segment. The position of the end of the second segment can be given as

$$\begin{bmatrix} x_2 \\ y_2 \\ z_2 \end{bmatrix} = \begin{bmatrix} r\cos(\theta_1) + h\cos(\theta_1)\sin(\theta_2) \\ r\sin(\theta_1) + h\sin(\theta_1)\sin(\theta_2) \\ h\cos(\theta_2) \end{bmatrix} \tag{9}$$

where r and h are the length of the first and second segment respectively. θ_1 and θ_2 are the rotation angle of the first and second joints. The Jacobian matrix $\boldsymbol{J}$ is then given as

$$\boldsymbol{J} = \begin{bmatrix} -\sin(\theta_1)(r + h\sin(\theta_2)) & -h\cos(\theta_1)\cos(\theta_2) \\ \cos(\theta_1)(r + h\sin(\theta_2)) & -h\sin(\theta_1)\cos(\theta_2) \\ 0 & h\sin(\theta_2) \end{bmatrix} \tag{10}$$

It can be seen in Eq. (10) that the Jacobian matrix loses its rank when $cos(\theta_2) = 0$ or $r + h\sin\theta_2 = 0$, which gives $\theta_2 = \pm 90°$ or $\theta_2 = sin^{-1}(-\frac{r}{h})$ if it exists. In both cases, the resultant angle exceeds the range of the pitch and yaw motion for TWrist, which indicates it is not subject to singularities within its workspace.

The analysis of the null space for TWrist is straightforward. Since it does not have redundant motion in any degree of freedom, TWrist does not exhibit a null space for specific postures. However, when multiple TWrists are cascaded to form a robot arm, the null space analysis aligns with that of conventional serial robot arms. Furthermore, given that each joint of TWrist provides multiple degrees of freedom, its null space is expected to be more enriched and complex compared to that of typical robot arms.

4.2. Compliance

As a robotic joint based on tensegrity structure, compliance is a key attribute of TWrist. To investigate this attribute, its passive stiffness was assessed. This is completed by measuring the extent of the TWrist prototype's externally induced bending in the pitch and yaw directions when a slowly varying radial external load is applied on it at a representative neutral posture, that is 0° for all its three rotational motions. The unique spatial irregularity of tensegrity structures, unlike conventional rigid-body joints, lacks easily accessible anchor points for attaching test equipment. To minimise measurement-induced perturbations, a trifurcated cable knot was introduced. A dynamometer, connected with the high longitudinal stiffness braided fishing line, was attached to cable knot at the central position of the top face of the upper prism, as shown in Fig. 10(a). The bending angle was measured using a method akin to that in the active workspace test. By concurrently recording data from both the dynamometer and the orientation sensor, a stiffness characteristic profile of the joint was delineated, as depicted in Fig. 10(b).

The results indicated that when TWrist experienced an angular displacement of 30°, the radial load applied at the centre of its top face was approximate 0.8 N m, corresponding to a counteracting torque output of the same value. The relationship between the induced angular displacement and the associated increase in load was not linear. Specifically, at angular displacements of 10° and 20°, the counteracting torques measured were approximate 0.2 N m and 0.45 N m, respectively. As the angles approached higher values, the required pulling force gradually increased, demonstrating high structural stability. Additionally, the motion responses for pitch and yaw exhibited similar characteristics. The results revealed that, in comparison to active motion scenarios, TWrist can readily reach and recover from larger bending angles under externally induced deformation. The departure and return trajectories of the tested pitch and yaw motions also formed a closed loop, which is consistent with active motions.

Notably, due to the constraints of the measurement approach, the stiffness in the roll motion was not evaluated in this study. Nevertheless, it is anticipated that the stiffness would significantly differ with and without the presence of active cables. In the relaxed state of the active cables, the roll motion exhibits reduced stiffness, primarily provided by arrangement of the cable guide slots of the central rod. When the active cables are fastened, the transition region exhibits substantial torsional resistance due to the active cables stiffness. However, the entire structure would remain compliant owing to the presence of the other tensegrity elements it is composed of.

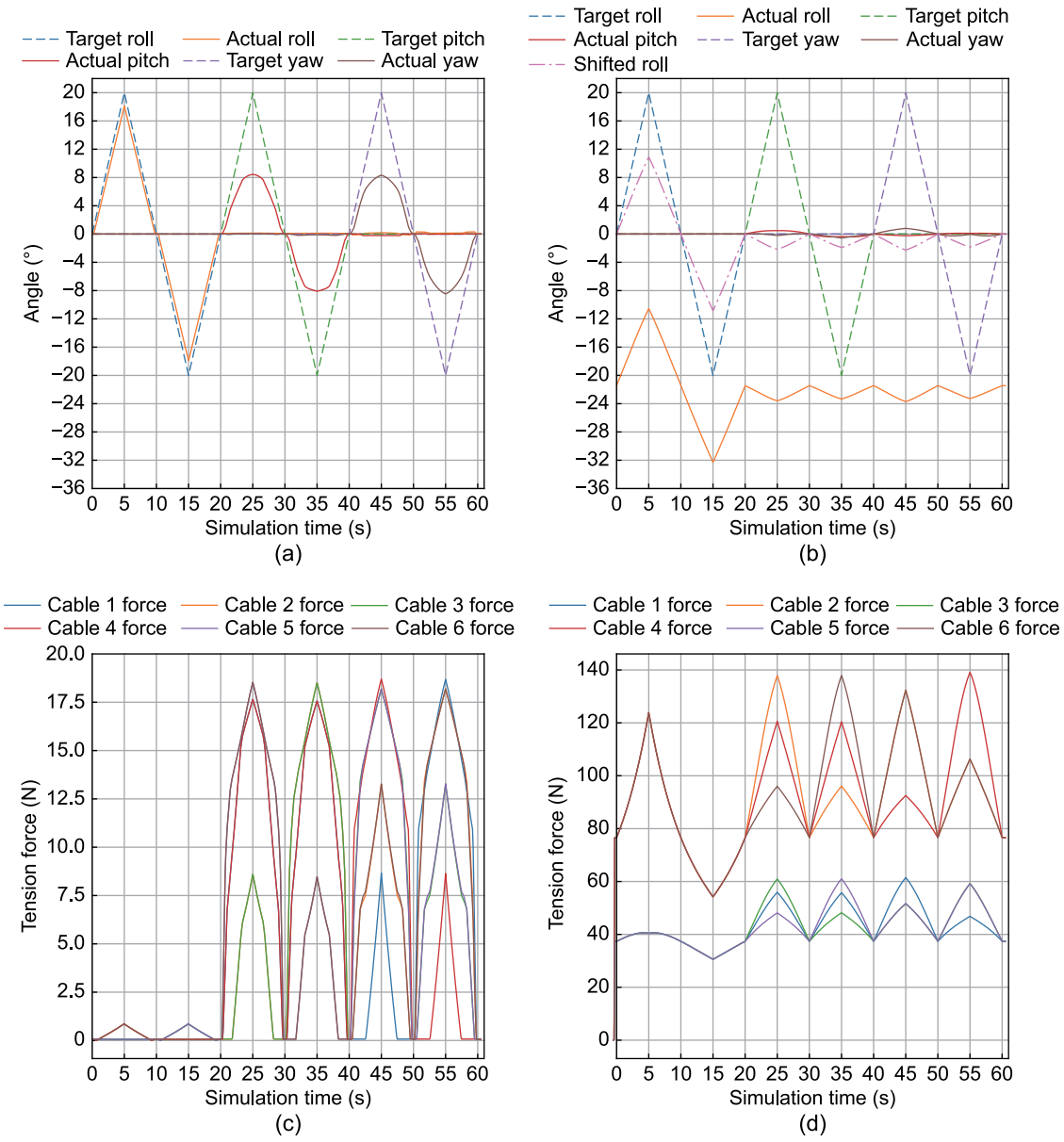

Fig. 11. The comparison results of TWrist and a typical tensegrity joint in simulation. (a) and (b) are the active workspace results of TWrist and the typical tensegrity joint respectively. The actual roll, depicted with the solid orange line, of the typical tensegrity joint shows a constant offset after the structure is pretensioned. A shifted roll data, depicted with the dash-dotted pink line, is plotted to cancel this offset for better illustration. (c) and (d) are the tension forces on the active cables for the target motion sequence in (a) and (b) respectively.

4.3. Agility

To assess the improvements in agility brought about by TWrist, a comparison was made with a typical stacked tensegrity joint in terms of active workspace and actuation inputs. The comparison was also carried out in simulation due to the lack of equipment for continuous measurement of the internal tension on the active cables.

For the control group, a typical two-stage tensegrity prism tower structure was constructed, as depicted in Fig. 6(b). This structure differs from TWrist as there is no central rod and the associated cables serving as the transition region. To maintain structural integrity, two sets of additional vertical cables were employed to connect the bottom and top nodes of the two prisms respectively. To ensure a consistent comparison, the heights where the two prisms overlap in the control group were matched to the separation distance between the two prisms in TWrist so that the length of the active cables are same at the neutral posture. The results, following the implementation of identical control algorithms and experimental procedures, are presented in Fig. 11.

When comparing the observed actuation ranges of TWrist with those of a typical tensegrity joint, TWrist demonstrates improved performance across all three rotational degrees of freedom, with increases of approximate 6.1°, 7.93° and 7.52°, or 51.3%, 1586% and 928% in percentage, in roll, pitch and yaw, respectively. Furthermore, the non-zero values of the actual roll motion during the pitch and yaw motions indicate that the asymmetry of the additional vertical cables in the typical tensegrity joint results in interference between pitch and yaw motions and the roll motion, validating previous concerns about the low controllability inherent in typical tensegrity structures. Additionally, when comparing the simulation results with practical experimental results for the TWrist prototype, it is evident that despite the inability of the simulation to capture real-world mechanical perturbations

and hysteresis, there is a reasonable consistency between the simulated and practical experimental results.

Regarding the results for cable tension, significant differences are observed as well. At a neutral posture, the active cables in the typical tensegrity joint are primarily engaged in maintaining structural integrity, where the essential pretension results in a constant static tension. Examining the maximum forces required, which represent the input from actuators to the structure, shows that TWrist reduces these demands by 123.12 N, 120.81 N and 113.76 N, corresponding to reductions of 99.3%, 87.63% and 85.88% for the roll, pitch and yaw motions, respectively. These findings highlight TWrist's lower torque requirements for actuators, enabling faster movements with the same actuator power. Together with a larger active workspace, these results emphasise the agility improvements that TWrist offers for tensegrity-based robotic joints than those based on regular stacked tensegrity structures.

5. Discussion

In addressing the challenges associated with motion efficiency and agility in tensegrity robots, this study introduces an intermediate stage into the cascaded tensegrity structure based on the under constrained transition region, a significant modification in tensegrity design. In conjunction with an actuation scheme inspired by the human antagonistic muscle pairs, it facilitates coordinated movement of the active cables by imitating the muscle contraction and relaxation. This methodology not only preserves structural integrity but also mitigates certain intrinsic motion constraints of conventional tensegrity frameworks. It simplifies the control complexity associated with multi-stage tensegrity systems, thereby unveiling improved 3-DoF active movement capabilities, especially in terms of the roll motion.

While TWrist offers improved movement capabilities as a robotic joint based on tensegrity principles, its operational workspace is relatively limited compared to conventional rigid-body rotational joints. An apparent solution is to increase the number of stages. It is worth mention that increasing the stage count in TWrist primarily serves to expand the collective workspace, rather than reducing the actuation resistance of tensegrity structures, which is different from the one mentioned in Section 1. However, the adaptation to a multi-stage configuration of TWrist can introduce potential complexities. For instance, adhering to the active cable routing scheme used in the 2-stage TWrist without incorporating additional actuators, each active cable needs to be routed through multiple cable guides over the course of the entire arm. This routing can induce hysteresis and unpredictability in the prism movements within the intermediate stages due to frictional forces. Take a three-stage robot arm configuration as an example, the prism in the second stage might not consistently align at half the total rotational angle, thereby disrupting the uniformity of structural properties across different stages. Furthermore, the challenge also escalates when each stage is endowed with independent motion control via additional actuators. A critical aspect here involves designing an effective cable routing strategy that enables actuation of the nth stage without hindering the movement of the $(n-1)th$ stage, thereby preserving the structure's external actuation scheme and maintaining minimal inertia at the end-effector.

As a robotic joint based on tensegrity structures, TWrist distinguishes itself through its compliance and flexibility. These characteristics, while advantageous, introduce complexities in compensating for external loads during its motion. In this study, its active workspace was only evaluated under no-load conditions, while the stiffness experiments highlight the compliance-related challenges. When an end-effector is attached to TWrist, or when it bears a load, both the workspace and motion accuracy will be significantly influenced as a result of the combined effects of gravity and the compliance. To address these motion discrepancies either with or without external loads in further research, one approach is to integrate visual servoing to provide real-time spatial positioning of the end-effector. This approach is anticipated to surpass the absolute orientation sensors employed in this study in terms of accuracy, information dimensions, and response time.

Another potential method is direct measurement of the cable lengths, for example, by determining the resistance of non-insulated cables, to compute the structure's actual posture through forward kinematics. This method, however, requires additional efforts to overcome measurement precision issues due to the inconsistency from instance to instance as a type of soft structure. Additionally, refining the control algorithms offers substantial promise. The control algorithm presented in this paper did not fully account for assembly-induced variances. It could potentially benefit from data-driven algorithms and calibration process to improve motion accuracy.

In addition to the compliance, flexibility and agility demonstrated by the experimental results in this paper, TWrist, a robotic joint based on tensegrity structures, also possesses advantages such as lightweight, stability, and fault tolerance. On the one hand, compared with conventional rigid joints, TWrist can be less vulnerable to external impacts, reduce the total weight of the system, and improve reliability. On the other hand, compared with robotic joints adopting a typical tensegrity structure, TWrist provides improved performance in terms of workspace, efficiency and agility, thus further narrowing the gap for practical applications of tensegrity in robotics. These characteristics are expected to play a crucial role in the scenarios outlined in Section 1. For example, in microgravity environments, given the reduced necessity for load compensation, its potential application as segments of the robot arm on orbital satellites, particularly in mitigating impacts from high-velocity space debris, is noteworthy. Moreover, its small end-effector inertia could mitigate the negative impacts of operational errors, further underscoring its suitability for space applications. In post-disaster scenarios, when TWrist is used for positioning the end-effector of a robot, such a flexible joint is not only beneficial in ensuring the functionality of the robot where collisions are common during operation, but also safer when interacting with humans on site. Given the larger motion range and the lower actuation requirements of the roll motion compared to the pitch and yaw motions, TWrist is particularly suitable to serve as the wrist joint in a robot arm, where three degrees of rotational freedom can be realised within a single joint to improve the agility of the end-effector.

The advantageous properties exhibited by TWrist indicate that introducing the design based on the under constrained transition region concept, coupled with a tailored control scheme, could substantially enhance the performance of tensegrity based robotic joints and tensegrity robots from multiple aspects, particularly in terms of agility. Contrary to prevailing mainstream approaches, the methodology proposed in this paper offers a novel perspective on the design of tensegrity robots. This method suggests moving beyond the highly redundant constraints inherent in tensegrity structures and instead retaining only essential constraints while allowing specific degrees of freedom. By integrating these degrees of freedom with specialised control algorithms, the overall performance of tensegrity robots can be systematically improved.

6. Conclusion

This paper presents the tensegrity robotic joint TWrist which innovatively adopts the under constrained transition region design to elevate the agility of the structure. The paper begins by outlining a design methodology that strategically increases motion freedom by selectively removing internal constraints in the tensegrity structure, while maintaining the structural integrity. The discussion then shifts to the leveraging of this enhanced maneuverability with the inherent compliance and flexibility of tensegrity, utilising these features with suitable control schemes.

Based on the proposed design framework, the study details the development of a 2-stage tensegrity robotic joint prototype complemented with essential driving peripherals, using an external actuation approach. Through inverse kinematics, the control algorithm for this joint is established. Experimental results demonstrate that TWrist can readily achieve three degrees of active rotational freedom based on typical tensegrity structures, coupled with evaluations of its active workspace and stiffness. The performance of this robotic joint reveals a promising approach to improve the agility of robotic joints and robots constructed with tensegrity structures. These insights are invaluable for advancing the future deployment and application of tensegrity robots in a broad range of scenarios.

CRediT authorship contribution statement

Tianyuan Wang: Conceptualization, Data curation, Formal analysis, Investigation, Methodology, Project administration, Resources, Software, Validation, Visualization, Writing – original draft, Writing – review & editing. **Mark A. Post:** Resources, Supervision, Writing – review & editing. **Andy M. Tyrrell:** Resources, Supervision, Writing – review & editing.

Declaration of competing interest

The authors declare that they have no known competing financial interests or personal relationships that could have appeared to influence the work reported in this paper.

Appendix A. Supplementary data

Supplementary material related to this article can be found online at https://doi.org/10.1016/j.birob.2024.100170.

References

[1] M.A. Post, X.-T. Yan, P. Letier, Modularity for the future in space robotics: A review, Acta Astronaut. 189 (2021) 530–547.
[2] J. Delmerico, S. Mintchev, A. Giusti, B. Gromov, K. Melo, T. Horvat, C. Cadena, M. Hutter, A. Ijspeert, D. Floreano, L.M. Gambardella, R. Siegwart, D. Scaramuzza, The current state and future outlook of rescue robotics, J. Field Robot. 36 (7) (2019) 1171–1191.
[3] C. Majidi, Soft robotics: A Perspective—Current trends and prospects for the future, Soft Robot. 1 (1) (2014) 5–11.
[4] C. Lee, M. Kim, Y.J. Kim, N. Hong, S. Ryu, H.J. Kim, S. Kim, Soft robot review, Int. J. Control Autom. Syst. 15 (1) (2017) 3–15.
[5] J. Lai, B. Lu, H.K. Chu, Variable-stiffness control of a dual-segment soft robot using depth vision, IEEE/ASME Trans. Mechatron. 27 (2) (2022) 1034–1045.
[6] A. Stilli, H.A. Wurdemann, K. Althoefer, A novel concept for safe, stiffness-controllable robot links, Soft Robot. 4 (1) (2017) 16–22.
[7] R.E. Skelton, J. William Helton, R. Adhikari, J.-P. Pinaud, W. Chan, An introduction to the mechanics of tensegrity structures, in: Y. Hurmuzlu, O.D.I. Nwokah (Eds.), The Mechanical Systems Design Handbook: Modeling, Measurement, and Control, CRC Press, 2002.
[8] R. Buckminster Fuller, R. Marks, The Dymaxion World of Buckminster Fuller, Anchor Books, Garden City, N.Y, 1973.
[9] K.D. Snelson, Continuous tension, discontinuous compression structures, 1965.
[10] R. Skelton, W.J. Helton, R. Adhikari, Mechanics of Tensegrity Beams, Rep (1998–1), UCSD, Structural Systems & Contr. Lab., 1998.
[11] M.C. Oliveira, R.E. Skelton, Tensegrity Systems, Springer, MA, 2009.
[12] S. Kaewunruen, C. Ngamkhanong, S. Xu, Large amplitude vibrations of imperfect spider web structures, Sci. Rep. 10 (1) (2020) 19161.
[13] F. Fraternali, N. Stehling, A. Amendola, B.A. Tiban Anrango, C. Holland, C. Rodenburg, Tensegrity modelling and the high toughness of spider dragline silk, Nanomaterials (Basel) 10 (8) (2020).
[14] N. Wang, K. Naruse, D. Stamenović, J.J. Fredberg, S.M. Mijailovich, I.M. Tolić-Nø rrelykke, T. Polte, R. Mannix, D.E. Ingber, Mechanical behavior in living cells consistent with the tensegrity model, Proc. Natl. Acad. Sci. USA 98 (14) (2001) 7765–7770.
[15] D.E. Ingber, Tensegrity I. Cell structure and hierarchical systems biology, J. Cell Sci. 116 (Pt 7) (2003) 1157–1173.
[16] S.M. Levin, 16. Tensegrity, the new biomechanics, in: M. Hutson, A. Ward (Eds.), Oxford Textbook of Musculoskeletal Medicine, Oxford University Press, 2016, pp. 155–156, 158–160.
[17] A.P. Sabelhaus, J. Bruce, K. Caluwaerts, P. Manovi, R.F. Firoozi, S. Dobi, A.M. Agogino, V. SunSpiral, System design and locomotion of SUPERball, an untethered tensegrity robot, in: 2015 IEEE International Conference on Robotics and Automation, ICRA, 2015, pp. 2867–2873.
[18] J. Bruce, K. Caluwaerts, A. Iscen, A.P. Sabelhaus, V. SunSpiral, Design and evolution of a modular tensegrity robot platform, in: 2014 IEEE International Conference on Robotics and Automation, ICRA, IEEE, 2014, pp. 3483–3489.
[19] J. Bruce, A.P. Sabelhaus, Y. Chen, D. Lu, K. Morse, S. Milam, K. Caluwaerts, A.M. Agogino, V. SunSpiral, SUPERball: Exploring tensegrities for planetary probes, in: International Symposium on Artificial Intelligence, Robotics and Automation in Space, I-SAIRAS, 2014.
[20] R. Kobayashi, H. Nabae, G. Endo, K. Suzumori, Soft tensegrity robot driven by thin artificial muscles for the exploration of unknown spatial configurations, IEEE Robot. Autom. Lett. 7 (2) (2022) 5349–5356.
[21] J. Kimber, Z. Ji, A. Petridou, T. Sipple, K. Barhydt, J. Boggs, L. Dosiek, J. Rieffel, Low-cost wireless modular soft tensegrity robots, in: 2019 2nd IEEE International Conference on Soft Robotics, RoboSoft, ieeexplore.ieee.org, 2019, pp. 88–93.
[22] J. Rieffel, J.-B. Mouret, Adaptive and resilient soft tensegrity robots, Soft Robot. 5 (3) (2018) 318–329.
[23] J. Friesen, A. Pogue, T. Bewley, M. de Oliveira, R. Skelton, V. Sunspiral, DuCTT: A tensegrity robot for exploring duct systems, in: 2014 IEEE International Conference on Robotics and Automation, ICRA, 2014, pp. 4222–4228.
[24] J.M. Friesen, P. Glick, M. Fanton, P. Manovi, A. Xydes, T. Bewley, V. Sunspiral, The second generation prototype of a duct climbing tensegrity robot, DuCTTv2, Proc. - IEEE Int. Conf. Robot. Autom. 2016-June (2016) 2123–2128.
[25] A.P. Sabelhaus, L.J. van Vuuren, A. Joshi, E.L. Zhu, H.J. Garnier, K.A. Sover, J. Navarro, A. Agogino, A. Agogino, Design, simulation, and testing of a flexible actuated spine for quadruped robots, 2018.
[26] R. Kobayashi, H. Nabae, K. Suzumori, Active-bending six-bar tensegrity modular robot driven by thin artificial muscles, IEEE Robot. Autom. Lett. (2023) 1–8.
[27] R. Kobayashi, H. Nabae, K. Suzumori, Large torsion thin artificial muscles tensegrity structure for twist manipulation, IEEE Robot. Autom. Lett. 8 (3) (2023) 1207–1214.
[28] B.R. Tietz, R.W. Carnahan, R.J. Bachmann, R.D. Quinn, V. SunSpiral, Tetraspine: Robust terrain handling on a tensegrity robot using central pattern generators, in: 2013 IEEE/ASME International Conference on Advanced Intelligent Mechatronics, 2013, pp. 261–267.
[29] D. Zappetti, S. Mintchev, J. Shintake, D. Floreano, Bio-inspired tensegrity soft modular robots, in: Biomimetic and Biohybrid Systems, Springer International Publishing, 2017, pp. 497–508.
[30] T. Kaufhold, F. Schale, V. Böhm, K. Zimmermann, Indoor locomotion experiments of a spherical mobile robot based on a tensegrity structure with curved compressed members, in: IEEE/ASME International Conference on Advanced Intelligent Mechatronics, AIM, 2017, pp. 523–528.
[31] F. Carreño, M.A. Post, Design of a novel wheeled tensegrity robot: a comparison of tensegrity concepts and a prototype for travelling air ducts, Robot. Biomim 5 (1) (2018) 1.
[32] T. Wang, in: M. Post, A. Tyrrell (Eds.), System Design for Modular Tensegrity Robots (Ph.D. thesis), School of Physics, Engineering and Technology, 2023.
[33] S. Lessard, D. Castro, W. Asper, S.D. Chopra, L.B. Baltaxe-Admony, M. Teodorescu, V. Sunspiral, A. Agogino, A bio-inspired tensegrity manipulator with multi-DOF, structurally compliant joints, in: 2016 IEEE/RSJ International Conference on Intelligent Robots and Systems, IROS, Vol. 2016-Noem, IEEE, 2016, pp. 5515–5520.
[34] J.M. Friesen, J.L. Dean, T. Bewley, V. Sunspiral, A tensegrity-inspired compliant 3-dof compliant joint, in: 2018 IEEE International Conference on Robotics and Automation, ICRA, IEEE, 2018, pp. 3301–3306.

[35] S. Ikemoto, K. Tsukamoto, Y. Yoshimitsu, Development of a modular tensegrity robot arm capable of continuous bending, Front. Robot. AI 8 (2021) 774253.
[36] D. Stewart, A platform with six degrees of freedom, Proc. Inst. Mech. Eng. 180 (1) (1965) 371–386.
[37] A. Tasora, R. Serban, H. Mazhar, A. Pazouki, D. Melanz, J. Fleischmann, M. Taylor, H. Sugiyama, D. Negrut, Chrono: An open source multi-physics dynamics engine, in: High Performance Computing in Science and Engineering, Springer International Publishing, 2016, pp. 19–49.
[38] M. Taylor, R. Serban, Validation of Basic Modeling Elements in Chrono, Tech. rep., University of Wisconsin-Madison, 2015.